Soft Matter

Ultrasonically synthesized organic liquid-filled chitosan microcapsules: Part 2: Characterization using AFM (Atomic Force Microscopy) and combined AFM-Confocal laser scanning fluorescence microscope

Journal:	*Soft Matter*
Manuscript ID	SM-ART-01-2018-000065.R2
Article Type:	Paper
Date Submitted by the Author:	14-Mar-2018

Complete List of Authors:	Mettu, Srinivas; University of Melbourne, Department of Chemical & Biomolecular Engineering Ye, Qianyu; University of Melbourne, Department of Chemical & Biomolecular Engineering Meifang, Zhou; University of Melbourne, Chemistry Dagastine, Raymond; The Univsersity of Melbourne, Chemical and Biomolecular Engineering Ashokkumar, Muthpandian; University of Melbourne, School of Chemistry;

Ultrasonically synthesized organic liquid-filled chitosan microcapsules: Part 2: Characterization using AFM (Atomic Force Microscopy) and combined AFM-Confocal laser scanning fluorescence microscope

Srinivas Mettu [*a,b], Qianyu Ye[a], Meifang Zhou[a], Raymond Dagastine[b], and Muthupandian Ashokkumar[a]

[a] School of Chemistry, The University of Melbourne, Parkville, Melbourne, Victoria 3010, Australia.
Fax: (+) 61 (3) 9347-5180, E-mail: masho@unimelb.edu.au, smettu@unimelb.edu.au Homepage: http://sono.chemistry.unimelb.edu.au/

[b] Department of Chemical Engineering, The University of Melbourne, Parkville, Melbourne, Victoria 3010, Australia.

KEYWORDS: · chitosan · ultrasound microcapsule · Atomic Force Microscopy (AFM) · stiffness · modulus · Laser Scanning Confocal Microscopy (LSCM)

Abstract:

Atomic Force Microscopy (AFM) is used to measure the stiffness and Young's modulus of individual microcapsules that have a chitosan cross linked shell encapsulating tetradecane. The oil filled microcapsules were prepared using one pot synthesis via ultrasonic emulsification of tetradecane and crosslinking of chitosan shell in aqueous solutions of acetic acid. The concentration of acetic acid in aqueous solutions of chitosan was varied from 0.2% to 25% v/v. The effect of acetic acid concentration and size of the individual microcapsules on the strength was probed. The deformations and forces required to rupture the microcapsules were also measured. Three dimensional deformations of microcapsules under large applied loads were obtained by the combination of Laser Scanning Confocal Microscope (LSCM) with Atomic Force Microscope (AFM). The stiffness and hence the modulus of the microcapsules was found to decrease with increase in size with the average stiffness ranging from 82 to 111 mN/m and average Young's modulus ranging from 0.4 to 6.5 MPa. The forces required to rupture the microcapsules varied from 150 to 250 nN with deformations of the microcapsules up to 62 to 110% relative to their radius, respectively. Three dimensional images obtained using laser scanning confocal microscope showed that the microcapsules retained their structure and shape after being subjected to large deformations and subsequent removal of the loads. Based on the above observations, the oil filled chitosan cross linked microcapsules are ideal choice for use in food and pharmaceutical industry as they would be able to withstand the process conditions encountered.

1 Introduction

Liquid filled microcapsules, where oil or water is encapsulated by cross-linked proteins [1-3], polymers [4-6] and various polysaccharides [7-12], have important functional properties. The microcapsules can be used in various industrial applications such as printing[13], textiles[14], agriculture[15], drug delivery[16, 17], heavy metal removal[18] and cartilage tissue engineering [19]. Other emerging areas where the use of such encapsulation techniques gaining importance are pharmaceutical and food industries[10, 20, 21]. Also, in functional food products, it may be necessary to deliver a flavor that is released in the mouth during the chewing process as well as a nutrient of active that must survive the chewing process and deliver the nutrients further along the digestive system. As it is the current practice in aroma delivery and more a potential application in processed foods, encapsulated materials may require less overall material to deliver a sensory perception or active benefit than mixing the material throughout a formulation or product. In addition, the encapsulation approach may also have advantages such as long shelf life, prevention of evaporation and oxidation of sensitive materials or blocking the unwanted interaction of encapsulated materials with other components in the product[20].

There have been various techniques developed to encapsulate liquids inside cross-linked shells. For example, layer-by-layer assembly [22], emulsion cross-linking [23] and ultrasound [7, 8]. Among these techniques, the ultrasound cross-linking method seems to be a suitable option for use in a range of industries including food and pharmaceutical. Ultrasonic synthesis does not use strong chemical cross-linkers and it is a one step process which can be easily scaled up in industrial setting. However, the stability and strength of the ultrasonically synthesized microcapsules needs to be carefully evaluated if they are to be embedded to into functional foods and pharmaceutical products. The shell must be non-porous so that encapsulates do not leak out during and after processing. In terms of the micro-mechanical properties of the cross-linked shell, it should have sufficient strength to survive the process conditions during the manufacturing or a product or formulation particularly in mixing processes as well as heating steps in food processing or sterilization, but still break or release the encapsulate at the desired point of delivery is a mechanical trigger for release is required. Hence the elasticity and rupture strength of the shell plays a significant role.

We have carried out mechanical compression experiments on a model microcapsule system that has a chitosan cross-linked shell encapsulating tetradecane. These microcapsules are synthesized by simultaneous emulsification of tetradecane into chitosan solution and cross-linking the chitosan shell using ultrasound. In part 1 of this paper, we reported details about the synthesis and stability of microcapsules prepared by varying the concentration of acetic acid from 0.2% to 25% v/v in the aqueous solutions of chitosan. In the current study, we carried out indentation experiments on individual microcapsules using Atomic Force Microscope (AFM). The aim of our study is to estimate the stiffness and strength of the cross-linked shell and the forces required to rupture them. Direct force measurement of nano- and micro-mechanical properties using AFM has been well utilized to measure the strength of individual non-porous air filled protein and lipid microcapsules and porous water filled polyelectrolyte and polymer microcapsules [24-36]. Unlike, the case of bulk rheology measurements where a compact bed of individual microcapsules or particles is subjected to stationary or oscillatory shear stresses using rheometers [37], the AFM can measure the stiffness and strength of an individual microcapsule. Force measurement on an individual microcapsule provides accurate estimate of the strength and more detailed information about the mechanics of microcapsules deformation compared to bulk rheology measurements. Also, the AFM can measure the strength of microcapsules as a function of their size. This information combined with process conditions that the microcapsule must been exposed to provide help define an optimum size required so that they do not break up during processing. Such a design information may not be available from bulk rheology measurements. In conjunction with AFM, we also used a laser scanning confocal fluorescence microscope to image and characterize the real-time deformation of a single microcapsule in 3-dimensions as it undergoes compression.

2 Materials

Chitosan and acetic acid (AA) were purchased from Sigma-Aldrich. Tetradecane (olefine free; >99%) was from Fluka. Milli-Q water was obtained from a Millipore system (18.2 MΩ/cm at 25°C). We reported details about the synthesis and stability of ultrasonically cross-linked chitosan microcapsules filled with tetradecane in part 1 of this paper. These microcapsules are prepared by varying the concentration of acetic acid from 0.2% to 25% in the aqueous solutions of chitosan. All glassware used in the

experiments was cleaned using Ajax detergent, soaking in Nitric Acid followed cleaning in base (NaOH), rinsed thoroughly with Milli-Q water and dried. Nitric Acid (Analytical Reagent grade 99%) was obtained from Ajax fine chemicals and used without purification.

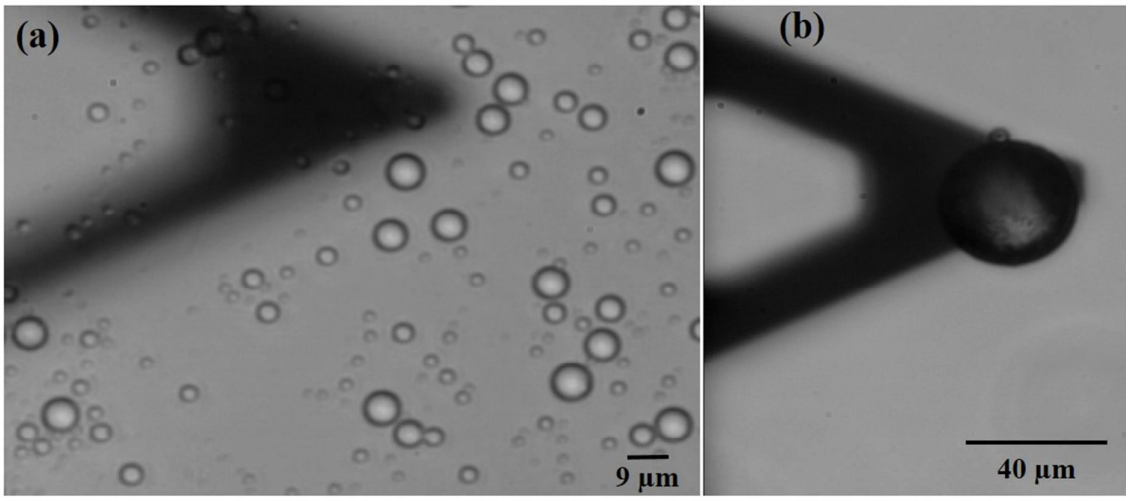

Figure 1: Optical microscope images of Chitosan microcapsules attached to plasma cleaned glass bottom of AFM Fluid Cell (a), Typical silica colloidal probe (b).

3 Experimental

3.1 Sample Preparation:

Ultrasonically cross-linked chitosan microcapsules filled with tetradecane were immobilized on circular glass substrates to carry out AFM indentation experiments. Four to five drops of concentrated suspension of microcapsules were added to acetic acid solution of pH~3 stored in a 10 ml plastic vial. Due to the low density, the capsules slowly cream up and float on top of the solution. The plastic vial was then filled up to the brim with addition of more acetic acid solution. The circular glass bottom of AFM fluid cell was first cleaned by soaking sequentially for an hour in detergent (Ajax), sodium hydroxide and concentrated nitric acid and washed with large amounts of milli-Q water and dried with ultra-purified nitrogen gas. The dried glass disks were then ozone cleaned (UV/Ozone ProCleaner Plus, Bioforce Nanosciences) for 20 minutes to remove any organic debris as well as to make the surface hydrophilic. The cleaned glass disks were then placed on top of the plastic vial containing microcapsules and left on the vial for about 24hrs. The microcapsules slowly cream up and firmly attach the glass slide

after 24 hrs. A typical optical microscope image of immobilized microcapsules along with the colloidal probe used to compress them is shown Figure 1.

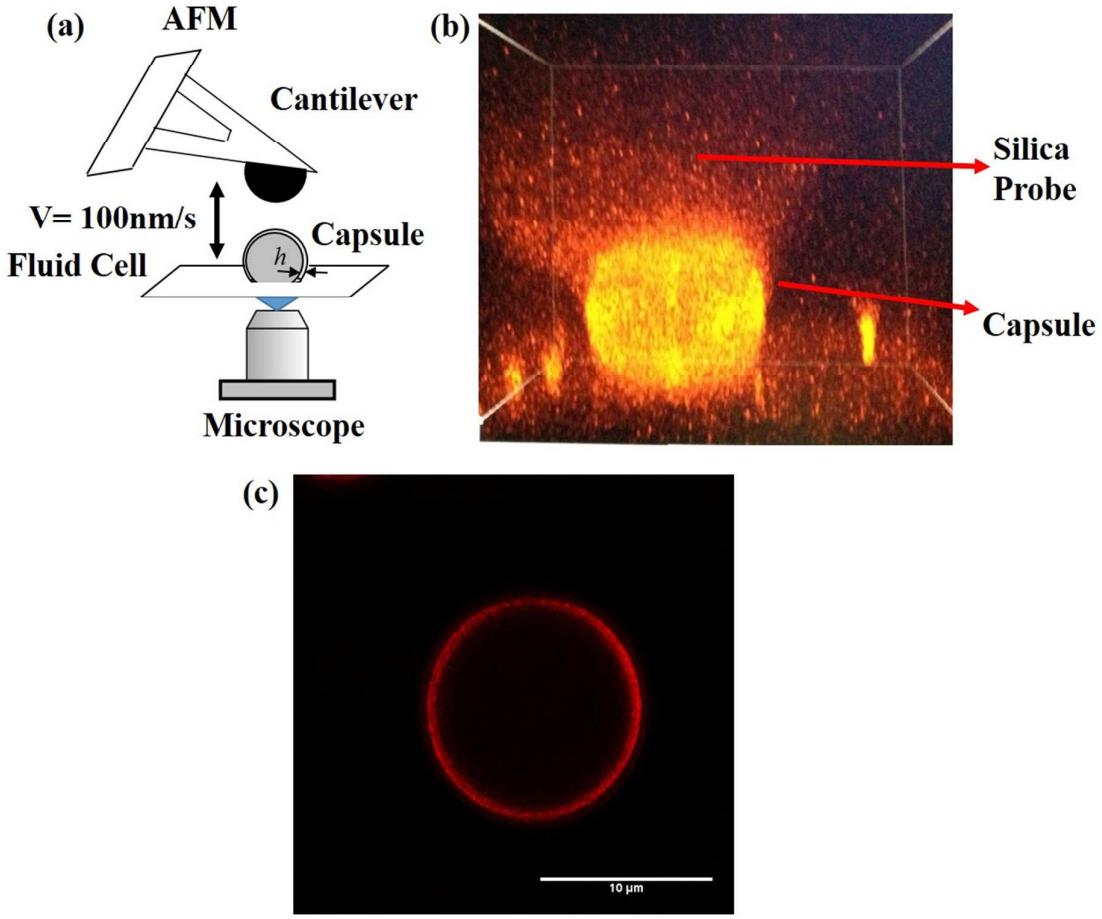

Figure 2. Schematic of the microcapsule indentation experiments carried out with AFM using a silica colloidal probe (a), 3-dimensional laser scanning confocal image of the actual experiment (b), 2-dimensional laser scanning image of the deformed microcapsule shown in (b) where the thin chitosan shell is identified by the bright red colour (c). The shell of the microcapsule was dyed with Rhodamine B. The diameter of the microcapsule is approximately 11.5 µm

Before carrying out the indentation experiments, the circular glass disk with microcapsules was attached to AFM fluid cell and 2 ml of pH~3 acetic acid solution was added fluid cell. Some of the capsules that were loosely anchored to the glass disk were dislodged with addition of acetic acid solution whereas microcapsules that were firmly anchored remained on the surface. The AFM fluid cell is then washed few times by addition and subsequent removal of acetic acid solution to remove any microcapsules that are floating in the fluid cell. The anchoring of microcapsules to glass bottom of AFM

fluid cell was further tested by adding 1 mL of acetic acid solution to the fluid cell while the microcapsules were observed with an inverted microscope (40X inverted microscope objective, Nikon Eclipse Ti-U). The microcapsules stayed anchored to glass bottom and were not dislodged (figure 1) with addition of more acetic acid solution. This observation indicated that there would be no slipping of microcapsules during compression with the silica colloidal probe in the AFM measurements.

3.2 AFM Indentation Experiments:

The silica colloidal probe used for indentation experiments (figure 2) was prepared by method described in Ducker et al[38] where a spherical colloidal silica particle was attached to V-shaped silicon nitride MLCT cantilevers (Bruker) by small amount of two part epoxy adhesive (from Super Glue Corp.) with 30 minute delayed setting time. In this method, a MLCT cantilever was lowered into a small amount of adhesive and then immediately, it is used to pick up a colloidal silica particle deposited on a glass slide. The cantilever with particle glued at the end was left at room temperature to allow the adhesive to dry and set for 24 hr. The diameters of the colloidal probe (silica particle) used for measuring the stiffness and modulus was constant around 20 μm whereas it ranged from 32 to 40 μm (figure 1 b) for probes used in rupture force experiments. The spring constant of the probes (measured by method of Hutter-Bechhoefer [39]) used for measuring the stiffness and modulus was around 0.1 N/m whereas it ranged from 0.4 to 0.55 N/m for probes used in rupture force experiments. Large spring constant (~0.5 N/m) probes were used for rupture force experiments to eliminate the non-linear bending of soft probes at high applied loads (~250 nN). AFM head was slowly lowered into the fluid cell containing microcapsules in pH~3 acetic acid solution to ensure that no air bubbles were trapped on the colloidal probe. Before carrying out indentation experiments on microcapsules, the sensitivity of colloidal probe was measured by acquiring a force curve between the bare glass of the fluid cell and the colloidal probe until a constant compliance region was achieved. The constant compliant region was used to calibrate the optical lever sensitivity. An example of the resulting force curve on the rigid glass substrate is shown in figure 3 (black filled circles). The individual microcapsules of appropriate size (>=4 μm) were located and the diameter was measured by recording an optical image with inverted microscope (40X objective, Nikon Eclipse Ti-U). The colloidal probe was then engaged and slowly

lowered onto to the microcapsule until a finite deflection of probe is recorded. The vertical alignment of colloidal probe with that of capsules is achieved further by adjusting the position of fluid cell (hence microcapsule) with a micromanipulation stage.

The microcapsule was then indented with colloidal probe by taking force-distance curves with a specified maximum applied force onto microcapsule. As all the AFM indentation experiments were carried in a fluid cell with aqueous solution, to eliminate hydrodynamic effects resulting from viscosity of acetic acid solution, all force-distance curves were obtained at velocities of 100 nm/s. The maximum force of indentation was fixed to approximately 10 nN. The indentation experiment was repeated 10 times on each microcapsule particle to check the reproducibility of the measurement. The diameter of the microcapsule showed no change through observation using the inverted microscope before and after the experiments. For each sample type, 10 to 12 different individual microcapsules were located on the glass surfaces and the indentation experiment was repeated on each of them. The force versus indentation data obtained on the microcapsules was analyzed using Reissner's theory [40, 41] as described in detail in later part of the article. Some adhesion was observed between the silica particle and microcapsules in the retraction portion of the force distance curve. Thus for the analysis of the elastic properties of the microcapsules, only the approach (indentation) portion of the force-distance curve was used to estimate the Young's modulus.

3.3 Combined AFM- 3-dimensional laser scanning confocal indentation:

A 3-dimensional laser scanning confocal image of the actual experiment is shown in figure 2 (b). For these experiments, the microcapsules were immobilized on an oxygen plasma treated fluorodish (World Precision Instruments Inc.) which is a cell culture petridish with glass bottom of 170 μm thickness. The thin glass bottom of fluorodish facilitates use of high magnification objectives (60x) that have short working distances in LSCM. We used Nanowizard II Bio AFM (JPK, give the COUNTRY!) mounted on a Nikon Eclipse Ti-E inverted microscope for the indentation experiments and Nikon A1Rsi laser scanning confocal microscope for 3-dimensional fluorescence imaging. For these experiments, the shell of the microcapsules was dyed with Rhodamine B. The indentation of microcapsule is carried out by applying a certain constant load ranging

from 105 nN and above on a microcapsule for a long time using the colloidal probe in constant force mode. While the microcapsule is under a constant applied load, the deformation the microcapsule deformation is captured through acquisition of a 3-D image by LSCM. We used a 561 nm laser to excite the dye and emission is collected in 638 nm channel. As a control, the microcapsule shape without any applied load were imaged. The images are then recorded at every 0.25 μm sections over the entire height of the microcapsule where reconstruction of the 2D slices give information about 3D image of how microcapsule deforms under applied load.

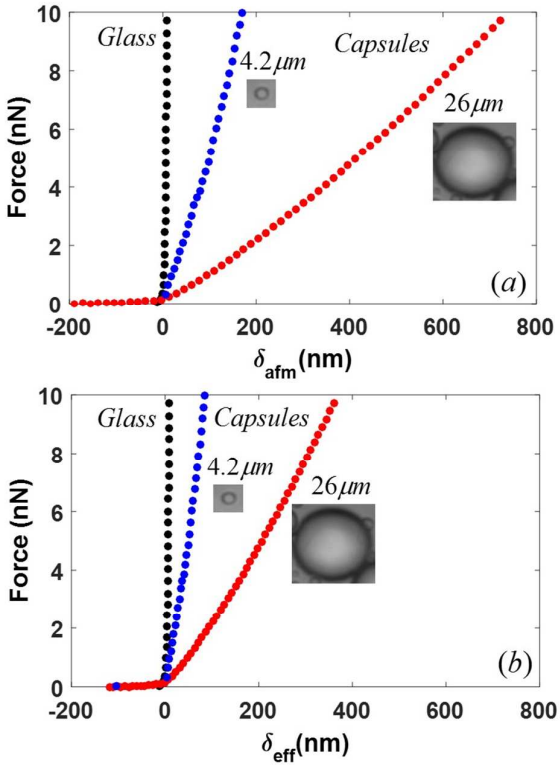

Figure 3. Determination of Young's modulus (E_s) from indentation experiments. Force versus measured indentation by AFM, δ_{afm} for microcapsules of 4.2 and 26 μm diameter. (Acetic acid concentration of 20 % v/v). (a), The effective indentation at the top of the microcapsules $\left(\delta_{eff} \sim 0.5\delta_{afm}\right)$ used for measuring the stiffness and modulus microcapsules (b). Stiffness of larger microcapsule is smaller. The black filled circles represent the force versus indentation curve against a glass surface given as a rigid reference substrate. The stiffness is calculated from the linear fit to the equation 3.

4 Qualitative discussion on the stiffness of microcapsules

Typical force versus indentation curves obtained using AFM are shown in figure 3 for a small (~ 4.2 μm) and a large (26 μm) microcapsule synthesized using an acetic acid concentration of 20%. The nearly vertical black filled circles shown in the figure is force versus indentation curve against a glass surface where no indentation was observed into the glass reference surface at these applied loads. However, in case of microcapsules which are highly deformable, indentation increases linearly with increase in applied load. The solid green lines show the approximate slopes of force curves. The microcapsules exhibit elastic behavior and no instabilities such as buckling or inflection of shell were observed with these applied loads. In these small deformation regime of thin shell indentation [40, 41], the slope of the force curve is proportional to the stiffness of the microcapsule and hence the modulus of the shell and the resistance of the microcapsule to deformation. As observed from figure 3, slope of the force curve decreased with an increase in the size of microcapsules. As shown in figure 4, we observed the reduction of stiffness with increase in diameter for all chitosan shelled microcapsules made with different amounts of acetic acid concentration ranging from 0.2 to 25%.

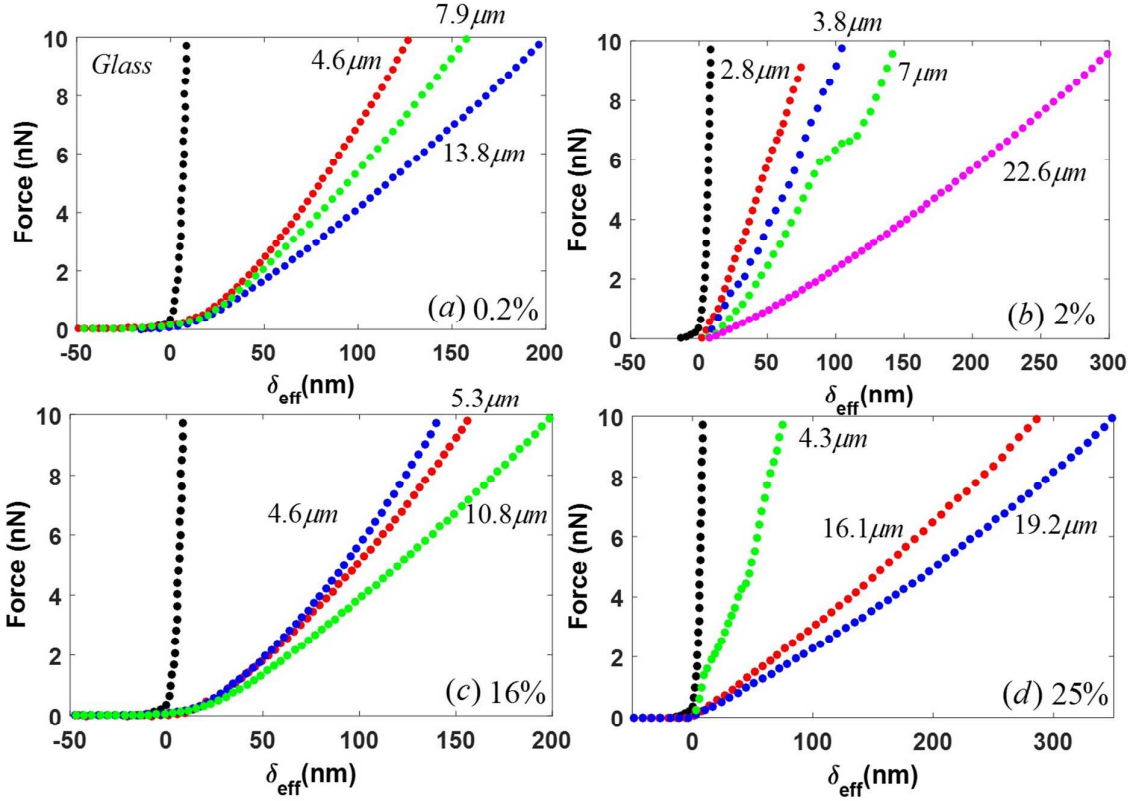

Figure 4. Force curves for effective indentation $(\delta_{eff} \sim 0.5\delta_{afm})$ of microcapsules as a function of diameter for microcapsules made with various acetic acid concentrations (%v/v). Corresponding acetic acid concentration is shown in each plot. The black filled circles represent the force versus indentation curve against a glass surface given as a rigid reference substrate.

5 Analysis of small micro-capsule deformation

In order to determine quantitative effects of amount of acetic acid and size of the microcapsules on stiffness and modulus, force versus indentation data was analyzed by using Reissner's theory [40, 41]. According to Reissner's theory, when a spherical microcapsule of radius R and shell thickness h is compressed by a rigid sphere of radius R_p at a given load F, the indentation (δ) of the microcapsule is related to applied load by

$$F = \left(\frac{4h^2}{R\sqrt{3(1-\nu^2)}} E_s \right) \delta \qquad (1)$$

where k_{shell} is the shell stiffness given by

$$k_{shell} = \frac{4h^2}{R\sqrt{3(1-\nu^2)}} E_s \qquad (2)$$

Here, E_s and R are modulus of the microcapsule and radius of the capsule. ν is the Poisson's ratio of microcapsule. We follow the notation that Rp and R are the radii of silica particle and microcapsule respectively whereas E_1 and E_s are their respective Young's modulus. Since silica particle is highly rigid (E_1~68 GPa) compared to microcapsules (E_s<7 MPa), its deformation is completely neglected.

Reissner's theory has frequently been applied to evaluate elasticity and stiffness of individual lipid, protein, polymer, hydrogel and polyelectrolyte capsules measured using AFM [24-34]. However, recently we have proposed[42] few modifications to Reissner's theory to account for the correct indentation of the microcapsules. When a solid particle[43] or microcapsule that is attached to a solid substrate is indented using a cantilever, the particle/microcapsule gets deformed at the top due to the load applied by the cantilever and at the bottom due to the presence of solid substrate. Hence, the indentation measured by AFM (δ_{afm}) is the sum of the indentation at the top (δ_{eff}) and

bottom (δ_s). For the correct use of equation 1, the effective indentation of the microcapsule at the top needs to be used (δ_{eff}). We found that the effective indentation is a function of radius of AFM probe (*Rp*), radius of microcapsule (*R*) and shell thickness (*h*). As there is no analytical solution to calculate effective indentation, we numerically obtained the correction factors to Reissner's theory as shown by the reformulation below.

$$F = \frac{4h^3}{R\sqrt{3(1-\nu^2)}} E_s \beta \left(C \frac{\delta_{afm}}{h} \right)^{\alpha} \qquad (3)$$

For a very large radius probe (*Rp/R*>>1) and small shell thickness (*h/R*<<1), the correction factor is C = 0.5 with β and α = 1. This corresponds to Reissner's theory with correction factor of 0.5 to equation 1 where there is an equal indentation of the microcapsule at the top and the bottom, the sum of which is equal to the indentation measured by AFM. For cases, other than limiting case shown above, the correction factors β, C and α are tabulated as a function of shell thickness, ratio of probe to capsule radius and Poisson ratio. We used corrected indentations to calculate our stiffness and modulus values. It is important to note that the above equations are valid only in the small deformation regime [24, 25]. In the cases where permeability of shells are unknown, it is suggested to measure the shell elasticity in the small deformation regime where the restoring force of the shell is proportional to the indentation. In the cases of impermeable shells, stretching of the shell membrane also contributes to the restoring force if the microcapsules are highly deformed. Hence in the large deformation regime, the volume constraint term due to membrane stretching that is proportional to cubic power of deformation needs to be considered. However, in our study, we restricted force maximum in the experiments to linear regime. The relative deformation $\varepsilon=\delta/2R$, in the experiments is in the order of the crossover deformation, $\varepsilon_{crossover} \sim \sqrt{h/4\pi R}$. For example, in the case of microcapsule of 10.8 μm diameter microcapsule prepared with 16% concentration of acetic acid that has a shell thickness *h* = 235 nm, $\varepsilon_{crossover}$~12 % deformation relative to the radius. The crossover deformation is approximately 635 nm. Hence, we find from figure 4 (c) that for force maximum of 10 nN, the deformation is in the linear regime only.

As observed from figures 3 and 4, for microcapsules synthesized using various amounts of acetic acid, F as a function of δ_{eff} is found to be linear. However, in many cases we observed that there was a nonlinear repulsive force behaviour observed within a nN of force. As these measurements were done in solution, we expect surface forces (electrical double layer etc) that cause repulsion between the tip and microcapsule. This is evident in figure 4 a and c for force curves obtained on microcapsules of different sizes. For example, in figure 4 a and c, within first 20 to 30 nm of indentation (< 1 nN force), the force curves are indistinguishable from each other even though the capsules sizes are very different (4.6 and 13.8 microns). In this region, we found that the force behaviour was not linear. Such a non-linear force repulsive behaviour could be resulting from surface forces or from the swollen polymer brushes of chitosan. Once this repulsive force region is overcome a linear force behaviour was observed. In such cases, we used linear region to estimate the shell stiffness. However, this is not observed in all cases. For example, in figure 4 b and d the difference in the slope of force curves for microcapsules of different sizes (2.8 to 7 microns) is clearly different from each other right from zero indentation. In such cases the shell stiffness is calculated right from zero indentation. The shell stiffness was regressed from the slope of the force curves ignoring the initial small non-linear region and the thickness of shell (h) was used calculate Young's modulus (E_s) according to equation (3). We used Poisson ratio of 0.4 as the correction factors β, C and α are available for this Poisson ratio.

Table 1. Average stiffness and Young's modulus of chitosan shelled microcapsules measured from AFM indentation experiments.

Sample Number	Acetic Acid Concentration (% V/V)	Average Shell thickness h (nm)	Average Stiffness k_{shell} (mN/m)	Average Modulus E_s (MPa)
2	0.2	134±10	82.2±16.4	6.5±1.2
20	2	511±73	71.4±30.5	0.4±0.1
160	16	235±35	83.5±15.3	1.9±0.3
200	20	207±94	96.2±40.7	3.1±0.7
250	25	150±24	111±67.5	6.0±0.8

The Young's modulus for microcapsules with varying concentration of acetic acid is listed in Table 1 along with their average stiffness. The average stiffness of microcapsules varied from 82 to 111 mN/m whereas the Young's modulus (E_s) varied from 0.4 to 6.5 MPa. The modulus values are in similar range or more than the values measured for air filled lysozyme cross linked microbubbles (E_s ~1.3 MPa). As observed from Table 1, the thickness of chitosan shell first increases with addition of acetic acid from 0.2 to 2% then decreases with a continued increase in acetic acid concentration. According to Reissner's theory, one would expect the microcapsule to be a convolution of Young's modulus, shell thickness and radius, thus the lack of a clear correlation between average stiffness and shell thickness may not be surprising. Whereas the Young's modulus shows an inverse proportional dependence on shell thickness, where the thickest shell was the lowest modulus. To further elucidate the dependence of microcapsule strength on thickness, one must examine the dependence of microcapsule strength with diameter.

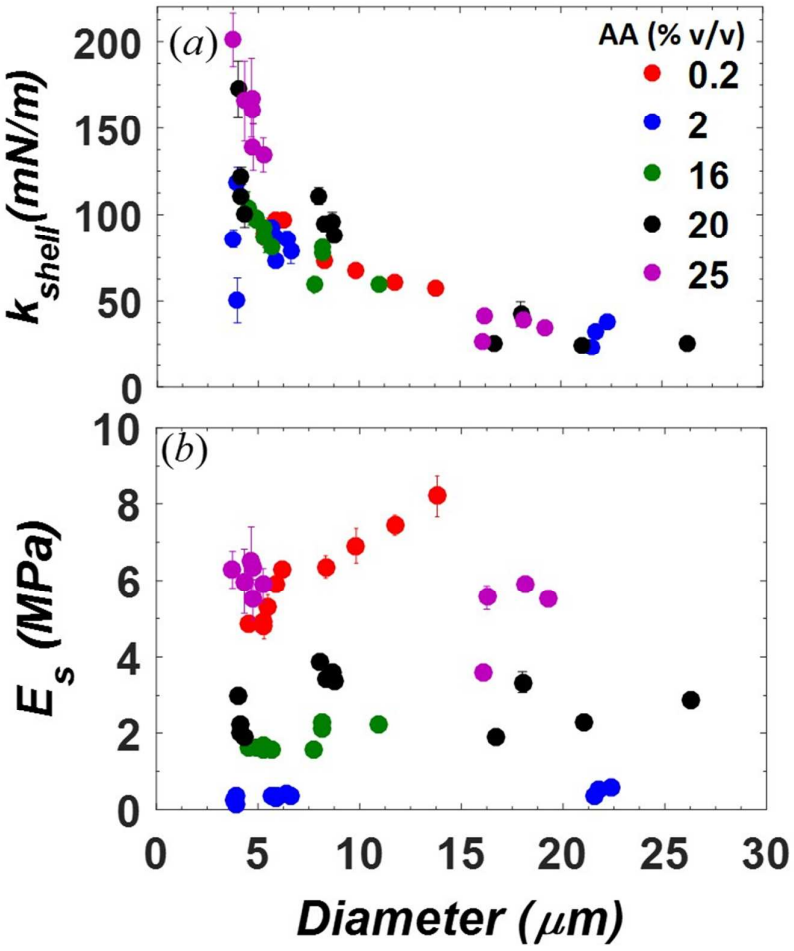

Figure 5. Stiffness (a) and Young's modulus (b) of chitosan cross linked tetradecane filled microcapsules as a function of microcapsule diameter at various concentrations of acetic acid. The stiffness of the microcapsules as a function of diameter falls onto a single curve at all concentrations of acetic acid.

As observed in figures 3 and 4, slope of the force curve was found to decrease with increase in the size for all chitosan shelled microcapsules made with different amounts of acetic acid concentration ranging from 0.2 to 25%. The stiffness data for individual microcapsules as a function of diameter in are shown figure 5 (a) synthesized at a range of acetic acid concentrations. The stiffness of microcapsules decreases by a factor 5 when the diameter increases from 5 to 27 μm. This observation of non-linear dependence of stiffness on diameter is in agreement with many single microcapsules compression experiments in the literature [29, 44-47]. The large stiffness at smaller diameters is the consequence of smaller radius of curvature and is consistent with equation 2. Such a decrease in stiffness of the microcapsules has significant implications for incorporation of these microcapsules into a formulated product and release. Smaller microcapsules may be more desirable to survive a shearing or chewing process, whereas large microcapsules may release more easily. Therefore, for a given shell material, for the large and small microcapsules to survive in shear flows and compressive stresses without rupturing, the size distribution needs to be properly tuned.

The measured modulus does not general show a dependence on microcapsule diameter in figure 5b. This is consistent with the model expectations described by Reissner's theory. The Young's modulus has a clear dependence on shell thickness, where the largest shell thickness (given in Table 1 or the inset in figure 5 a) has the lowest modules magnitude. This is also correlated to the non-monotonic dependence of the acetic acid concentration during the synthesis of the microcapsules. These modulus data further support the expectation that the acetic acid concentration affects the chitosan denaturation, adsorption and subsequent cross linking of the chitosan shell during synthesis in a complex manner, discussed in the mechanism discussion in part 1 of this study.

In comparing these measurements of microcapsule strength to literature values of similar chitosan materials, the only data available was for a chitosan microcapsule

that was not cross-linked. A study on the strength of chitosan coated (but not cross linked) DOPC vesicles using AFM is by Rinaudo et al[34] who found that the chitosan coated vesicles strength was higher than bare uncoated vesicles. However, as the chitosan was not cross-linked in their study, the stiffness and modulus of chitosan-coated vesicle was much less compared to cross-linked chitosan microcapsules in our study. For example, Rinaudo et al [34] found that a 4 μm diameter chitosan coated vesicle deforms 30 % relative to its diameter when subjected to 3 nN force, whereas as observed in our study as shown in figure 4 (b), a 3.8 μm diameter chitosan cross linked microcapsule deforms 5% relative to its diameter when subjected to a high force of 10 nN. These observations clearly indicate that chitosan cross-linking due to ultrasound increased strength of the shell.

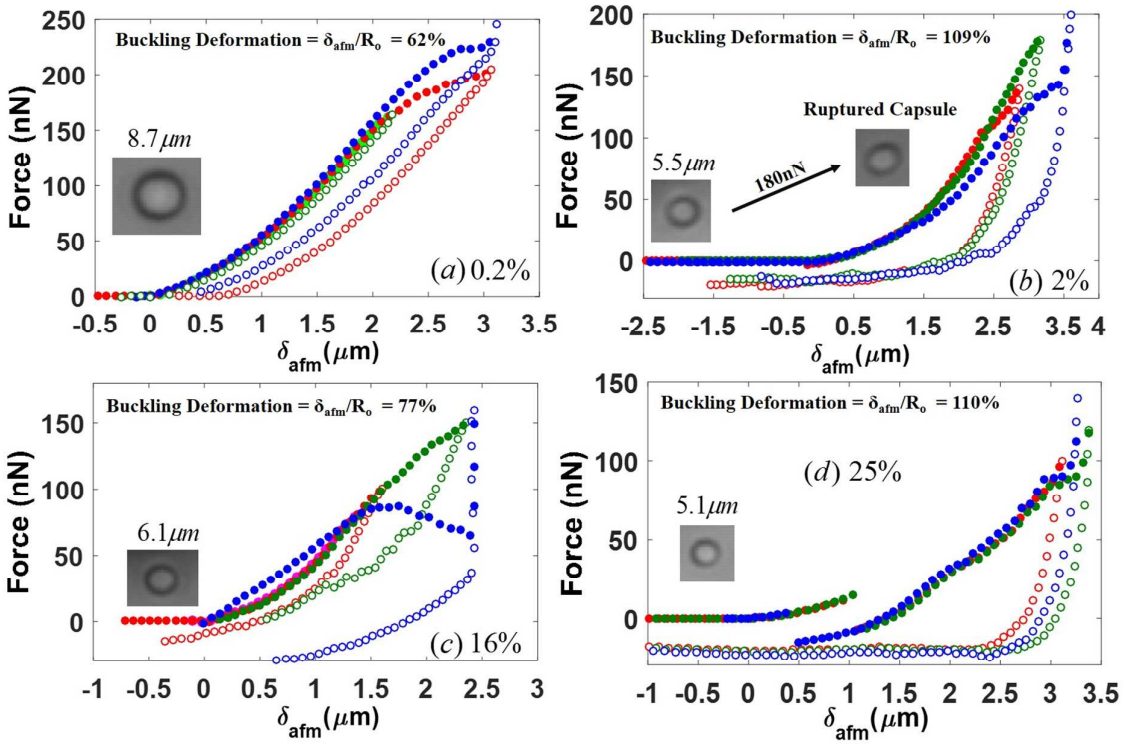

Figure 6. Deformation at rupture force for various samples as a function of acetic acid concentrations (%v/v). Corresponding acetic acid concentration is shown in each plot. The closed and open symbols correspond to the extension and retraction part of the indentation experiments respectively. The force curves are taken on an individual microcapsule with successive increase in force maximum until buckling and hence rupture event is recorded. Various colours indicate these successive force curves on the same individual microcapsule. The maximum force to which the microcapsule is subjected to varied from 10 to 250 nN.

However, for the clarity of presentation only few force curves are shown with different colours.

6 Rupture force experiments.

To correlate the strength of microcapsules to the rupture force required to break the microcapsules in shear flow during processing or from compressive stresses during incorporation into a solid material, the maximum applied force and deformation that the microcapsules survive can survive was measured. AFM indentation measurements were carried out on microcapsules by successively increasing the force maximum to approximately 250 nN. The force curves thus obtained on the chitosan cross-linked microcapsules for various acetic acid concentrations are shown in figure 6. The closed symbols correspond to extension part of the force curve whereas the open symbols correspond to the retraction part. Prior to reaching applied loads where microcapsule buckling occurs, the blue curves in Figures 6, a,b,c, and d, the increase in applied force for successive three force curves, the red and green curves, lead to an increase in the hysteresis between extension and retraction force curves. This indicates that in small deformation regime, only the elastic nature of the cross-linked shells is probed hence underlying tetradecane was unlikely to have a significant effect on the force measurement. At these large forces and deformations it is expected that both the bending and stretching moments of the shell material will become important to the microcapsule response, but the hysteresis in the approach and retract suggests physical changes to the microcapsule occurs which may include possible breaking of crosslinks, re-arrangement the chitosan, or a contribution to the response of from the oil due to the constant volume constraint of the oil drop and the adsorption of the chitosan to the oil-water interface of the microcapsule increases. At the point of buckling, (solid blue symbols in figure 6), a discontinuity is often observed between the approach and retract curves and subsequent measurements show little to no increase in force in response to deformation. An optical microscope image of a broken microcapsules is shown in figure 6 (b) where the shape of the capsule is non-spherical. When a hollow or a gas filled, microcapsule breaks with applied load, the colloidal probe comes directly in contact with the underlying glass substrate resulting in the constant compliance region like the force curve on a glass substrate as shown in figure 3 (black filled circles) of the manuscript. However, the chitosan microcapsules in our study are not hollow but filled

with oil (Tetradecane). After the rupture of microcapsule shell, underlying oil prevents the colloidal probe contacting the glass substrate. Hence we did not observe any constant compliance region after the rupture which is expected only for hollow or gas filled microcapsules. As we found that after the rupture event there was no force response from the ruptured capsule for subsequent indentation experiment. These observations clearly indicate that the microcapsules ruptured as observed from force discontinuities. Hollow or gas filled microcapsules that are well studied in literature that are made with synthetic polymers undergo plastic deformation when subjected to large loads and retain their non-spherical shape with the subsequent removal of load without rupturing. However, in our study the microcapsules are filled with tetradecane encapsulated by biopolymer chitosan shell. In this case, the microcapsule can retain its spherical shape even after undergoing plastic deformation due to the presence of oil and its surface tension effects. However, when the oil filled microcapsule ruptures, the oil sticks to the glass substrate resulting in non-spherical shape of ejected oil drop. We found that the ruptured capsules always have non-spherical shape as opposed to intact capsules that always have spherical shape.

The maximum force at each microcapsule buckles and ruptures depends both the porosity and thickness of the shell. For example, as we have shown in part 1 of this paper, the shell of chitosan microcapsules prepared with 0.2% acetic acid had a smaller force relaxation hence smaller porosity compared to microcapsule prepared with 25% acetic acid. As shown in figures 6 (a) and (d), microcapsule corresponding 0.2% acetic acid buckles at 62% deformation relative its radius while microcapsule corresponding to 25% acetic acid buckles at 110% deformation even though the shell thicknesses of these microcapsules are of the same order (Table 1). In the case of small shell thickness with less porosity, at large deformations the applied energy is not dissipated in inducing flow through pores but utilized in stretching the membrane and ultimately resulting in its rupture. However, if the shell is porous, it can with stand large applied forces and hence large deformations without rupturing. Chitosan cross linked microcapsules made with 25% acetic acid buckle only when the deformation reaches above 110% relative to its radius. As observed for microcapsule made with 2% acetic acid that had a large shell thickness of 511 nm, it can with stand 109% deformation before it buckles (figure 6 (b)). The microcapsules made with 16% acetic acid that had a shell thickness of 235 nm

buckled when the deformation reached above 77% (figure 6 (c)). We found that these microcapsules had porous shell as observed from stress relaxation experiments (data not shown). The stress relaxation behavior on these microcapsules can be analyzed using semi-analytical and finite element models developed by Hu et al [48, 49] to calculate permeability and porosity of the cross linked chitosan network.

7 3D imaging of microcapsule deformation

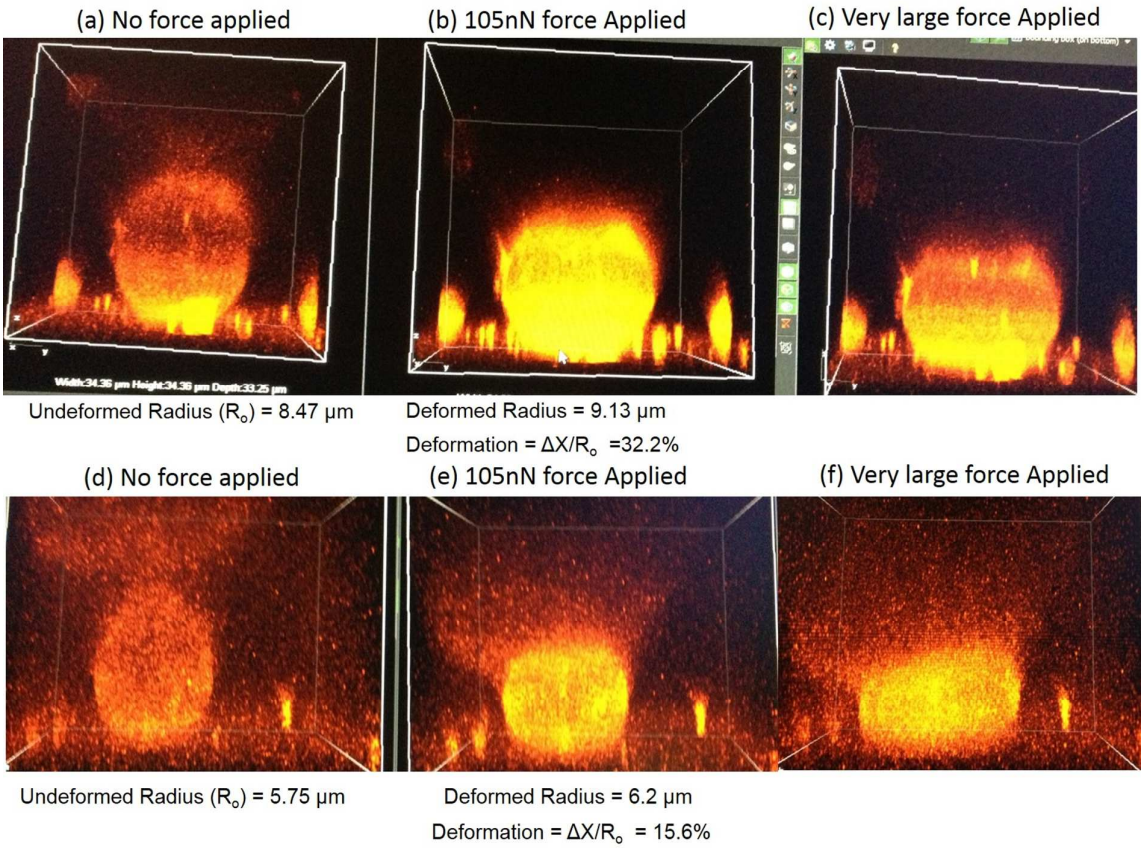

Figure 7. 3D deformation of microcapsules under no load (a, d), 105 nN force (b, e) and a very large force (c, f). The bulging of the oil filled microcapsule is evident with subsequent increase in load from left to right. Animated 3D deformation movies of microcapsules corresponding to top row are provided in supplemental information.

In order to visualize how the microcapsules deform under large applied loads, a combined AFM indentation experiments was carried out while imaging their 3 dimensional deformation using Laser Scanning Confocal Microscope (LSCM) simultaneously as schematically shown in figure 2[50, 51]. Three dimensional LSCM images at various applied loads are shown in figure 7 for two different chitosan cross-linked

microcapsules made by 25% acetic acid. The bulging of tetradecane filled microcapsules is evident with increase in applied load from no load to very large load. However, the microcapsules do not break with large applied loads. The microcapsules under no load look like they are stretched which is due to the self-lensing effect as suggested by Tan et al[50] and Tabor et al[51]. It was observed that the fluorescence in the chitosan shell gets slowly bleached under illumination from the excitation lasers. To show high contrast image at high loads, imaging was started for the microcapsules at a 105 nN applied load. The applied load was increased to a very high value that could not be measured due to the limitation of force range of the cantilever used in Nanowizard II Bio AFM. The large load on the microcapsules was applied by moving the colloidal probe onto the microcapsule by few microns using the step motor of the AFM. The microcapsule was unloaded and imaged under no applied load. Hence, the fluorescence intensity in the images decreased from 105 nN load to no load condition. This order of experiments also helped in confirming that the microcapsules were stable even after they were subjected to large deformations. As shown in figure 7 (b), the microcapsule survives more than 32% deformation without breaking. Animated 3-dimensional deformation movies of capsules corresponding to figure 7 (a), (b) and (c) are provided in supplemental information. Microcapsules under very large applied load as shown in figure 7 (f) survive more than 50% deformation without breaking. These observations in conjunctions with rupture force measurements clearly indicate the microcapsules might survive the shear and deformations encountered in processing conditions in pharmaceutical industries. 2D scans at every 0.25 μm section can be analyzed to measure intensity of emission from dye to obtain deformation as show in figure 8. The 2D section shown in the figure is taken from approximately middle portion of the microcapsule. The shell of the microcapsule is circular under no load (figure 8 (a)) and deforms with a 105 nN load (figure 8 (b)) and looks like an oval. The amount of deformation can be obtained from measuring the fluorescence intensity across the image as shown in figure 8 (c). The deformation information thus obtained can be used to validate the predicted shape of the microcapsules using detailed modeling of the microcapsules using large deformation theories [35, 52, 53].

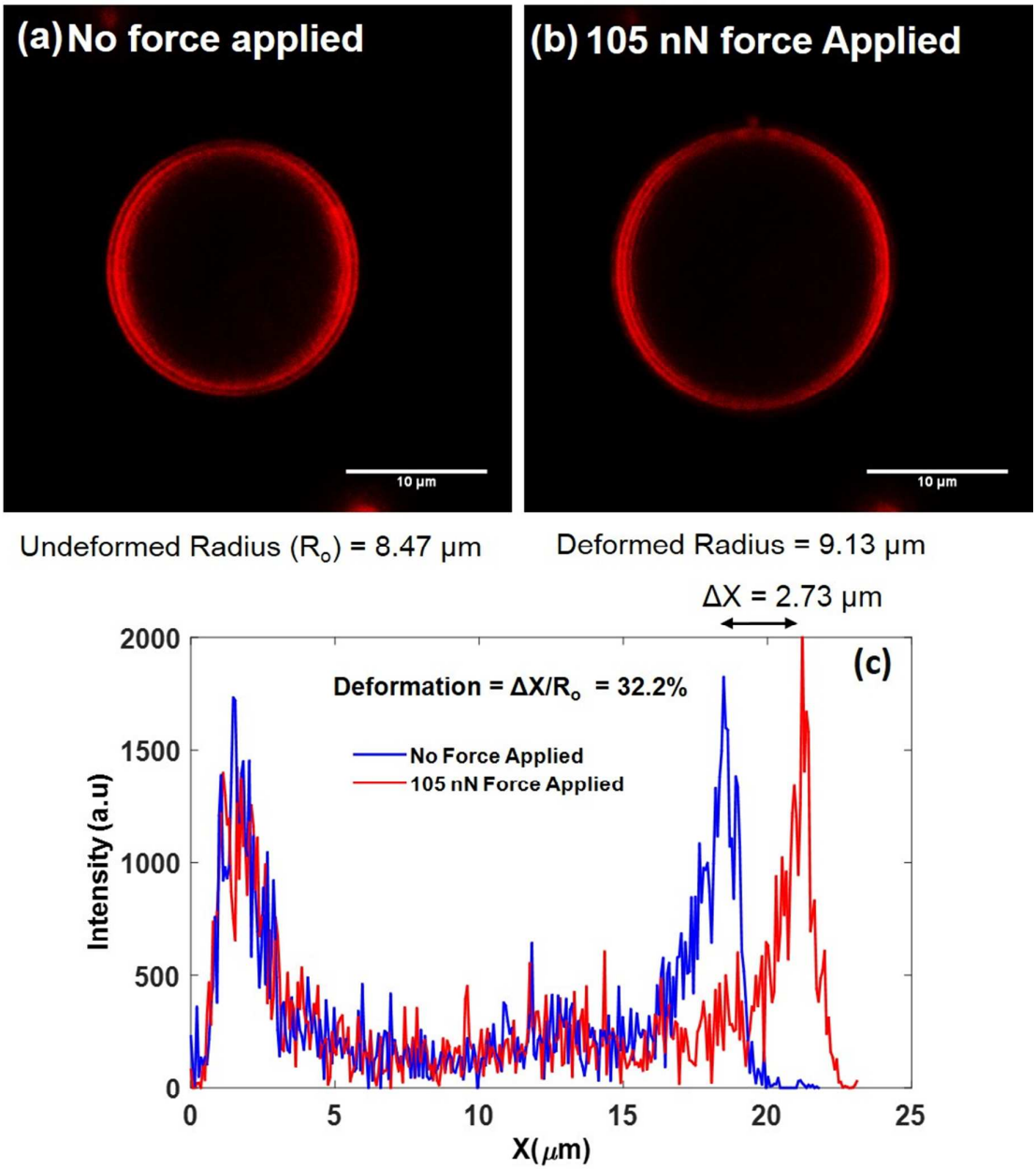

Figure 8. 2D slices at the center of the microcapsule under no load and 105 nN force (top). The emission intensity used to measure the deformation of microcapsule at the center section (bottom). The microcapsule deforms about 32 % of its radius with 105 nN applied load.

8 Conclusions:

The stiffness and Young's modulus of ultrasonically synthesized chitosan cross linked tetradecane filled individual microcapsules using Atomic Force Microscope (AFM) synthesized at a range of acetic acid concentrations in solution. The effect of acetic acid concentration on the stiffness and modulus was quantified. The stiffness and modulus was also measured as a function of diameter of the individual microcapsules. The stiffness of microcapsules decreased with increase in size where the measured average stiffness of microcapsules varied from 82 to 111 mN/m whereas average Young's modulus varied from 0.4 to 6.5 MPa and was less dependence on microcapsule diameter. The dependence of the shell thickness and the Young's modulus of the acetic acid concentration of the microcapsule synthesis conditions indicate that the differences in amount of chitosan and crosslinking that occur in the shell formation directly impact the ultimate strength of the shell material.

The forces required to rupture the microcapsules varied from 150 to 250 nN that correspond to 62 to 110% deformation of the microcapsules relative to their radius. The magnitude of rupture forces correlated well with stress relaxation behavior of the microcapsules as presented in part 1 of this paper. Based such high relative deformations that the microcapsules could with stand, we expect that these microcapsules would be able to survive high deformations and compressive stresses encountered during processing conditions in pharmaceutical industry. The 3-dimensional deformation of the individual microcapsules were measured using combined Laser Scanning Confocal Microscope (LSCM) and Atomic Force Microscope (AFM). The encapsulated tetradecane did not leak and microcapsules could retain their shape after application and subsequent removal large applied loads below the microcapsules buckling point.

Acknowledgements:

We thank the Australian Research Council (ARC), The University of Melbourne and Mondelez Australia for providing funding through Industrial Transformation Research Hub (ITRH, Project ID: IH120100053) and the PFPC for providing infrastructure support. We also thank Dr. John Zhu and Dr. Hemayet Uddin at Melbourne Center for Nanofabrication (MCN) for their help in the combined Laser Scanning Confocal

Microscope (LSCM) and AFM experiments. This work was performed in part at the Melbourne Centre for Nanofabrication (MCN) in the Victorian Node of the Australian National Fabrication Facility (ANFF) and in the Materials Characterization and Fabrication Platform (MCFP) at the University of Melbourne.

Conflicts of Interest:

There are no conflicts to declare.

AUTHOR INFORMATION

Corresponding Author

Srinivas Mettu (smettu@unimelb.edu.au)

Author Contributions

The manuscript was written through contributions of all authors. All authors have given approval to the final version of the manuscript.

Funding Sources

Australian Research Council (ARC), The University of Melbourne and Mondelez Australia through Industrial Transformation Research Hub (ITRH, Project ID: IH120100053).

9 References

1. K. S. Suslick and M. W. Grinstaff, *Journal of the American Chemical Society*, 1990, **112**, 7807-7809.
2. K. Suslick, M. Grinstaff, K. Kolbeck and M. Wong, *Ultrasonics Sonochemistry*, 1994, **1**, S65-S68.
3. M. Zhou, T. S. H. Leong, S. Melino, F. Cavalieri, S. Kentish and M. Ashokkumar, *Ultrasonics sonochemistry*, 2010, **17**, 333-337.
4. G. Paradossi, F. Cavalieri, E. Chiessi, V. Ponassi and V. Martorana, *Biomacromolecules*, 2002, **3**, 1255-1262.
5. P. Fernandes, M. Pretzl, A. Fery, G. Tzvetkov and R. Fink, in *Ultrasound Contrast Agents*, eds. G. Paradossi, P. Pellegretti and A. Trucco, Springer Milan, 2010, DOI: 10.1007/978-88-470-1494-7_9, ch. 9, pp. 109-127.
6. B. M. Teo, M. Ashokkumar and F. Grieser, *Physical Chemistry Chemical Physics*, 2011, **13**, 4095-4102.
7. E. Colombo, F. Cavalieri and M. Ashokkumar, *ACS applied materials & interfaces*, 2015.
8. M. Zhou, B. Babgi, S. Gupta, F. Cavalieri, Y. Alghamdi, M. Aksu and M. Ashokkumar, *RSC Advances*, 2015, **5**, 20265-20269.

9. M. Carin, D. Barthès-Biesel, F. Edwards-Lévy, C. Postel and D. C. Andrei, *Biotechnology and bioengineering*, 2003, **82**, 207-212.
10. A. H. King, 1988.
11. L. Liu, J.-P. Yang, X.-J. Ju, R. Xie, Y.-M. Liu, W. Wang, J.-J. Zhang, C. H. Niu and L.-Y. Chu, *Soft Matter*, 2011, **7**, 4821-4827.
12. W. Klaypradit and Y.-W. Huang, *LWT-Food Science and Technology*, 2008, **41**, 1133-1139.
13. B. K. Green, *Journal*, 1955.
14. G. Nelson, *International Journal of Pharmaceutics*, 2002, **242**, 55-62.
15. K. Tsuji, *Journal of microencapsulation*, 2001, **18**, 137-147.
16. B. B. C. Youan, T. L. Jackson, L. Dickens, C. Hernandez and G. Owusu-Ababio, *Journal of controlled release*, 2001, **76**, 313-326.
17. X. Zou, X. Zhao, L. Ye, Q. Wang and H. Li, *Journal of Industrial and Engineering Chemistry*, 2015, **21**, 1389-1397.
18. J. He, Y. Lu and G. Luo, *Chemical Engineering Journal*, 2014, **244**, 202-208.
19. S. E. Kim, J. H. Park, Y. W. Cho, H. Chung, S. Y. Jeong, E. B. Lee and I. C. Kwon, *Journal of controlled Release*, 2003, **91**, 365-374.
20. R. Arshady, *Journal of Microencapsulation*, 1993, **10**, 413-435.
21. N. J. Zuidam and E. Shimoni, in *Encapsulation technologies for active food ingredients and food processing*, Springer, 2010, pp. 3-29.
22. C. Lu, B. Mu and P. Liu, *Colloids and Surfaces B: Biointerfaces*, 2011, **83**, 254-259.
23. E. Biró, A. S. Németh, T. Feczkó, J. Tóth, C. Sisak and J. Gyenis, *Chemical Engineering and Processing: Process Intensification*, 2009, **48**, 771-779.
24. A. Fery, F. Dubreuil and H. Möhwald, *New journal of Physics*, 2004, **6**, 18.
25. M. P. Neubauer, M. Poehlmann and A. Fery, *Advances in colloid and interface science*, 2014, **207**, 65-80.
26. N. Elsner, F. Dubreuil, R. Weinkamer, M. Wasicek, F. Fischer and A. Fery, in *Characterization of Polymer Surfaces and Thin Films*, Springer, 2006, pp. 117-123.
27. A. Fery and R. Weinkamer, *Polymer*, 2007, **48**, 7221-7235.
28. C. Picart, B. Senger, K. Sengupta, F. Dubreuil and A. Fery, *Colloids and Surfaces A: Physicochemical and Engineering Aspects*, 2007, **303**, 30-36.
29. M. Pretzl, M. Neubauer, M. Tekaat, C. Kunert, C. Kuttner, G. r. Leon, D. Berthier, P. Erni, L. Ouali and A. Fery, *ACS applied materials & interfaces*, 2012, **4**, 2940-2948.
30. F. Cavalieri, J. P. Best, C. Perez, J. Tu, F. Caruso, T. J. Matula and M. Ashokkumar, *ACS applied materials & interfaces*, 2013, **5**, 10920-10925.
31. E. Buchner Santos, J. K. Morris, E. Glynos, V. Sboros and V. Koutsos, *Langmuir : the ACS journal of surfaces and colloids*, 2012, **28**, 5753-5760.
32. J. P. Best, M. P. Neubauer, S. Javed, H. H. Dam, A. Fery and F. Caruso, *Langmuir : the ACS journal of surfaces and colloids*, 2013, **29**, 9814-9823.
33. R. H. Abou-Saleh, S. A. Peyman, K. Critchley, S. D. Evans and N. H. Thomson, *Langmuir : the ACS journal of surfaces and colloids*, 2013, **29**, 4096-4103.
34. M. Rinaudo, F. Quemeneur, F. Dubreuil, A. Fery and B. Pépin-Donat, *International Journal of Polymer Analysis and Characterization*, 2013, **18**, 617-626.
35. K. Liu, D. Williams and B. Briscoe, *Physical Review E*, 1996, **54**, 6673.
36. C. Wang, J. Pritchard and C. Thomas, *Journal of texture studies*, 2006, **37**, 597-606.
37. N. M. Pinkerton, S. W. Zhang, R. L. Youngblood, D. Gao, S. Li, B. R. Benson, J. Anthony, H. A. Stone, P. J. Sinko and R. K. Prud'homme, *Biomacromolecules*, 2013, **15**, 252-261.
38. W. A. Ducker, T. J. Senden and R. M. Pashley, 1991.
39. J. L. Hutter and J. Bechhoefer, *Review of Scientific Instruments*, 1993, **64**, 1868-1873.

40. E. Reissner, *Journal of Mathematics and Physics*, 1946, **25**, 80-85.
41. E. Reissner, *Journal of Mathematics and Physics*, 1946, **25**, 279-300.
42. J. D. Berry, S. Mettu and R. R. Dagastine, *Soft Matter*, 2017, **13**, 1943-1947.
43. M. Glaubitz, N. Medvedev, D. Pussak, L. Hartmann, S. Schmidt, C. A. Helm and M. Delcea, *Soft Matter*, 2014, **10**, 6732-6741.
44. C. C. Chen, S.-Y. Wu, J. D. Finan, B. Morrison and E. Konofagou, *Ultrasonics, Ferroelectrics, and Frequency Control, IEEE Transactions on*, 2013, **60**, 524-534.
45. E. Glynos, V. Koutsos, W. N. McDicken, C. M. Moran, S. D. Pye, J. A. Ross and V. Sboros, *Langmuir : the ACS journal of surfaces and colloids*, 2009, **25**, 7514-7522.
46. J.-M. Gorce, M. Arditi and M. Schneider, *Investigative radiology*, 2000, **35**, 661-671.
47. V. Sboros, E. Glynos, S. Pye, C. Moran, M. Butler, J. Ross, W. McDicken and V. Koutsos, *Ultrasonics*, 2007, **46**, 349-354.
48. Y. Hu, X. Zhao, J. J. Vlassak and Z. Suo, *Applied Physics Letters*, 2010, **96**, 121904.
49. X. Zhao, N. Huebsch, D. J. Mooney and Z. Suo, *Journal of applied physics*, 2010, **107**, 063509.
50. S.-Y. Tan, R. F. Tabor, L. Ong, G. W. Stevens and R. R. Dagastine, *Soft Matter*, 2012, **8**, 3112-3121.
51. R. F. Tabor, H. Lockie, D. Mair, R. Manica, D. Y. C. Chan, F. Grieser and R. R. Dagastine, *The Journal of Physical Chemistry Letters*, 2011, **2**, 961-965.
52. P. Pujara and T. Lardner, *Zeitschrift für angewandte Mathematik und Physik ZAMP*, 1978, **29**, 315-327.
53. W. Feng and W.-H. Yang, *Journal of Applied Mechanics*, 1973, **40**, 209-214.